CSIRO PUBLISHING

International Journal of Wildland Fire **2016**, *25*, 229–241
http://dx.doi.org/10.1071/WF13178

A comparison of level set and marker methods for the simulation of wildland fire front propagation

Anthony S. Bova[A], *William E. Mell*[B,D,E] *and Chad M. Hoffman*[C]

[A]CPP, Inc., 2400 Midpoint Drive, Suite 190, Fort Collins, CO 80525, USA.
[B]US Forest Service, Pacific Wildland Fire Sciences Laboratory, 400 North 34th Street, Suite 201, Seattle, WA 98103, USA.
[C]Warner College of Natural Resources, Forest and Rangeland Stewardship, Colorado State University, 1472 Campus Delivery, Fort Collins, CO 80523, USA.
[D]Present address: Pacific Wildland Fire Sciences Laboratory, US Forest Service, 400 N 34th Street, Suite 201, Seattle, WA 98103, USA.
[E]Corresponding author. Email: wemell@fs.fed.us

Abstract. Simulating an advancing fire front may be achieved within a Lagrangian or Eulerian framework. In the former, independently moving markers are connected to form a fire front, whereas in the latter, values representing the moving front are calculated at points within a fixed grid. Despite a mathematical equivalence between the two methods, it is not clear that both will produce the same results when implemented numerically. Here, we describe simulations of fire spread created using a level set Eulerian approach (as implemented in the wildland–urban interface fire dynamics simulator, WFDS) and a marker method (as implemented in FARSITE). Simulations of surface fire spread, in two different fuels and over domains of increasing topographical complexity, are compared to evaluate the difference in outcomes between the two models. The differences between the results of the two models are minor, especially compared with the uncertainties inherent in the modelling of fire spread.

Additional keyword: WFDS.

Received 15 October 2013, accepted 25 August 2015, published online 16 November 2015

Introduction and background

Physics-based models of wildland fire processes can be used to conduct 'numerical experiments' that allow researchers to study fire behaviour and effects over a wide range of spatial and temporal scales. However, such models are computationally demanding and generally cannot give results at operational (faster than real time) time scales. In contrast, estimates of fire front propagation can be generated faster than real time by using empirical models based on relatively simple formulae that incorporate relevant parameters such as wind speed, slope and fuel properties. An example of such a model is the FARSITE package available from the US Forest Service, which uses the Rothermel model (Rothermel 1972) of fire spread, as implemented in Behave, and assumptions about fire front geometry to estimate and graphically illustrate the spread of a fire front across a given landscape (Finney 2004).

In describing the motion of a fire front, an observer can focus on the changes that take place at given points in space as the front passes, or on what happens while following the points comprising the moving front. These frames of reference are referred to as Eulerian and Lagrangian respectively (see e.g. Kundu and Cohen 2008). A moving fire front can be modelled from the perspective of either of these frames. For example, the FARSITE model computes the movement of separate Lagrangian points, also called vertices or markers, that are connected to form a fire front. Although it is a valid approach, it has two computational disadvantages. First, as the modelled fire front expands, the number of connected markers that form the front must increase in order to maintain an accurate shape. More significantly, modelling the crossing of separate fronts, or separate sections of the same front, requires considerable bookkeeping and computational time to determine which points represent burned and unburned areas (Sethian 1997; Finney 2004).

An Eulerian alternative to the marker approach is the 'level set' method of tracking an interface, where the Lagrangian perspective is exchanged with the Eulerian via a relatively simple mathematical transformation (Sethian 1992). An advantage of this method is that the behaviour of merging fronts arises naturally from the underlying mathematics and thus does not require the special handling that is needed when a marker method is used (Rehm and McDermott 2009).

The viability of the level set method for modelling fire spread has been established by several authors. Using a fire spread model created by Fendell and Wolff (2001), Mallet *et al.* developed a level set model that demonstrated the ability of the method to simulate the merger of separate fire fronts and the

closure of 'islands' of unburned fuel (Mallet *et al.* 2009). As mentioned, these phenomena pose computational difficulties for Lagrangian models of fire spread. Mandel *et al.* integrated a level set fire spread model with the Weather Research and Forecasting (WRF) model (Mandel *et al.* 2011). Although rates of fire spread and fire power (often, but erroneously, referred to as heat release rate (Quintiere 2006)) are calculated using the Rothermel equations, their model allows for fire–atmosphere interaction on spatial scales of tens of metres. Details of this model are also discussed in Coen (2013). Lautenberger developed a level set model containing the same elliptical fire spread model found in FARSITE (Lautenberger 2012). This model used topographical and fuel data from actual terrain in a mountainous area of northern California to create realistic fire spread patterns for hypothetical fires.

Two papers provide limited examinations of the similarities between the results of level set and Lagrangian simulations, and each employs identical fire spread models. Barber *et al.* (2008) created a level set model for comparison with the Canadian fire spread model, Prometheus, a Lagrangian fire spread simulator that contains an elliptical fire shape model similar to that found in FARSITE. Fire contours created using the level set model were very similar to those of the Lagrangian model. However, only one fire spread case over a flat terrain was used in the comparison, and it did not include the crossing or merging of fire lines. Rehm and McDermott (2009) compared the results of fire spread simulations from a level set model with those of a Lagrangian model that utilised the method of lines (MOL). Two simulation scenarios, in which the initial ignition pattern was a line and a circle respectively were compared for a flat terrain. The different models gave very similar, but not identical, results. In fact, it is to be expected (Rehm and McDermott 2009) that the two approaches will give different results, owing to the approximations made in their numerical implementation (e.g. time-step size, number of markers in the Lagrangian approach, spatial resolution in the Eulerian approach). This is likely to be more evident as the complexity of fuel and slope conditions and fire line interaction increases.

The goal of this paper is to address the lack of comparisons between simulations utilising the level set and marker methods. To evaluate the similarity of results between the two methods, we compared corresponding surface fire spread simulations, of increasing topographical and fuel complexity, generated by a level set model and by FARSITE. The level set algorithm was implemented in the wildland–urban interface (WUI) Fire Dynamics Simulator (WFDS), which contains both a physics-based (WFDS-PB) model for fire behaviour simulations (Mell *et al.* 2007) and an approach for fire front propagation based on the level set method (WFDS-LS). In the following text, WFDS-LS will be abbreviated to LS. The same elliptical spread model used in FARSITE (FS) was implemented in the LS model in order to ensure consistency between the models. The LS fire front propagation model can be coupled to WFDS-PB to account for terrain-shaped wind fields and fire–atmosphere interaction through the presence of a simple heat source at the location of the fire line. This coupling is easily implemented because the same computational grid can be used for the level set and the physics-based model. However, the most direct comparison with FS is to assume a constant wind speed and direction, which is the approach taken here and does not require a coupling between the level set and physics-based components of WFDS. Therefore, this paper presents work that is a first step towards a more complete testing of the implications of this lack of dynamic coupling. A summary of the level set method and results of these comparisons are described below.

The level set method can be easily understood by metaphor. Consider an ideal, circular front expanding uniformly outward in a Cartesian plane over time. Another way to imagine this circle is to consider a conical cup filling with water. The set of points at the level surface of the water where it meets the inner surface of the cup will form an expanding circle over time. In this example, the cup represents a level set function, $\phi_{LS}(x, y, t)$, that defines a height above or below a point (x, y) at a given time, t. The zero level set in a plane cutting through the cup comprises the points on the cup surface at which $\phi_{LS} = 0$. Virtually any shape of the front is possible. For example, filling a tilted cup would result in an expanding ellipse, and one can imagine water filling a much more complex and convoluted shape, resulting in multiple, irregular fronts. Fortunately, such a shape does not need to be known beforehand in order to model an evolving front using the level set method. Instead, a partial differential equation for the level set function is created and numerically solved.

In the Lagrangian framework, the position of a marker can be indicated by the coordinates $(x(t), y(t))$, where x and y are functions of time. Because this marker is a part of the front, and, as in the example above, the value of the level set function at the front is defined by zero, we can write the level set function as $\phi_{LS} = f[x(t), y(t), t] = 0$ (Sethian 1997). To transform this to an Eulerian framework, we find the rate of change of the level set function at a fixed point, $d\phi_{LS}/dt$, by the chain rule of calculus:

$$\frac{d\phi_{LS}}{dt} = \frac{\partial\phi_{LS}}{\partial t} + \frac{\partial\phi_{LS}}{\partial x}\frac{dx}{dt} + \frac{\partial\phi_{LS}}{\partial y}\frac{dy}{dt} = 0$$

where the arguments of ϕ_{LS} have been suppressed for clarity. Note that $\partial x/\partial t$ and $\partial y/\partial t$ may be rewritten, in the context of this paper, as rates of fire spread:

$$\frac{d\phi_{LS}}{dt} = \frac{\partial\phi_{LS}}{\partial t} + R_u\frac{\partial\phi_{LS}}{\partial x} + R_v\frac{\partial\phi_{LS}}{\partial y} = 0 \qquad (1)$$

where R_u and R_v are rates of spread in the x- and y-directions, respectively.

Eqn 1 can be solved numerically given initial and boundary values of ϕ_{LS} in the simulation domain, as well as values, or a model, of the rate(s) of fire spread, R_u and R_v. The zero-wind, zero-slope head fire spread rate, R_0, in the LS routine was provided by the BEHAVE model (Andrews 2014). Modification of R_0 to account for non-zero wind and slope is identical in LS and FS (see Appendix 1). Rates of spread of the flanking and backing portions of the front are estimated using the same equations found in FS, where it is assumed that the fire front has an elliptical shape with an empirically derived length-to-breadth ratio (Anderson 1983). Details of the level set model and the numerical solution methods may also be found in Rehm and McDermott (2009).

Methods

Simulations with identical configurations were executed using LS (i.e. the level set, Eulerian-based approach in WFDS) and FS

Table 1. Fuel models
n/a, not applicable

Fuel model	Packing ratio β (·)	Surface area to volume ratio σ (m^{-1})	Fuel height h (m)	1-h fuel moisture M1 (%)	10-h fuel moisture M10 (%)	100-h fuel moisture M100 (%)	Live herbaceous fuel moisture LHM (%)	Live woody fuel moisture LWM (%)	No-wind, no-slope rate of spread R_0 ($m\ s^{-1}$)
Old chamise (15)	0.0041	3344	0.91	2	4	5	90	70	0.007
Custom grass	0.0012	11 400	0.51	6	n/a	n/a	n/a	n/a	0.04

(i.e. the marker, Lagrangian-based approach in FARSITE) and the results compared. An active domain with horizontal dimensions of 1 × 1 km was used in all simulations. Except for a few cases described below, the LS domain was discretised as a mesh comprising 10 × 10-m cells. With the exception of simulations of fire spread on flat terrain, the vertical resolution (Δz) in the LS simulations was 1 m. In all LS simulations, an unignitable perimeter 100 m wide was maintained around the active domain to ensure constant boundary conditions during the simulation. Slopes in LS are calculated from the differences in height of neighbouring obstructions that form topography or landscape features. As in FS, the effect of slope on the length-to-breadth ratio (LTBR) (and, consequently, the head-to-flank ratio) of an elliptical fire front is estimated in LS by calculating an *effective* wind speed that gives the same rate of spread as the combination of slope and prescribed wind speed. The effective wind speed is then used to calculate the LTBR.

No-wind, no-slope rates of spread, R_0, for input into the LS model were calculated using BEHAVE software (the Rothermel (1972) rate of spread model that is the basis of BEHAVE is currently not incorporated into LS). Details of the calculation of midflame wind speed for the LS model are given in Appendix 1.

In LS, a flux-limiting scheme is used as part of the numerical solution of Eqn 1. Flux limiters, also called 'slope limiters', essentially add a correction to first-order upwinding in order to smooth solutions in non-linear systems (Ferziger and Peric 2002). Three flux-limiter functions – first-order upwinding, minmod and superbee – are available in LS. These functions and the flux-limiting method are described in Rehm and McDermott (2009). Unless stated otherwise, the (default) min-mod limiter was employed. Technical details related to the implementation of the elliptical-spread model and the numerical solution of the level set equation are given in Appendix 1.

Fuel, slope and aspect data in FS were described in grid-ASCII format with 10-m resolution (i.e. 100 × 100 data points) and the fire-line perimeter (distance between vertices) was set to a maximum of 10 m.

Two different surface fuel models were used, separately and together, in the LS and FS simulations. A grassland fuel model was created with attributes similar to those of *Eriachne burkittii* (kerosene grass), as described in Mell *et al*. (2007). In addition, US Forest Service (USFS) custom model 15 (old chamise) was used in several simulations (Weise and Regelbrugge 1997). Hereafter, these fuel models will be referred to as 'grass' and 'chamise' respectively. Identical fuel attributes were used in the LS and FS simulations (Table 1).

Topography, wind speed and direction, fuel parameters and ignition locations were matched as closely as possible between the LS and FS models. No fire acceleration (i.e. no change in rate between ignition and steady-state spread) was implemented in either model.

To compare the respective LS and FS simulations, isochrones of the time of arrival (TOA) of fire lines were compared. In LS, the TOA at a grid point is the first time-step at which the value of the level set function at that point is greater than or equal to zero (see Appendix 1). In practice, no points in the domain will be exactly equal to zero at a given time-step; therefore, the TOA will have an uncertainty equal to one time-step, which, in turn, corresponds to a few metres' uncertainty in the spatial location of the TOA. This uncertainty is negligible on the scale of the plotted isochrones.

The isochrones (TOA contours) were compared using a custom Matlab® (Mathworks, Inc., v. 2010, Natick, MA) script that estimates the lengths of fire perimeters and burned areas at periodic intervals.

Results: comparing the level set and FARSITE simulations

Simple cases: point ignitions on flat terrain

Fig. 1*a* illustrates the results of LS and FS simulations of fire spread over flat terrain with custom grass fuel and wind flowing left to right with a speed of 18 km h^{-1}. Ignition was located at the point with the (x, y) coordinates of (250 m, 500 m) in the simulations. The contours indicate the positions of the fire fronts of the LS (black) and FS (grey) models at 180-s intervals. The rate of change of the perimeters and burned areas are identical between the two models. The models also produced identical results when the wind speed was increased to 26 km h^{-1} (not shown).

Repeating the above case with a wind speed of 18 km h^{-1}, but with two separate ignition points, it is apparent that the merging of fire lines is nearly identical between the two models (Fig. 1*b*). In this case, the fire lines first meet ~540 s into the simulations. There is a very slight difference in the appearance of the corresponding contours in this region (near $x = 300$ m, $y = 500$ m), as the LS model gives a somewhat more resolved merging pattern (note the very small unburned island in the LS contour at that particular point and time-step). Regardless, the later contours overlap almost perfectly. Both models also gave matching results when the chamise fuel was used within the same domain and for the same parameters and when the terrain had a constant slope (not shown).

Adding complexity: fuel transitions and breaks

To provide a varied pattern of fuel transitions, 100 × 100-m patches of chamise or grass fuel were randomly placed in the

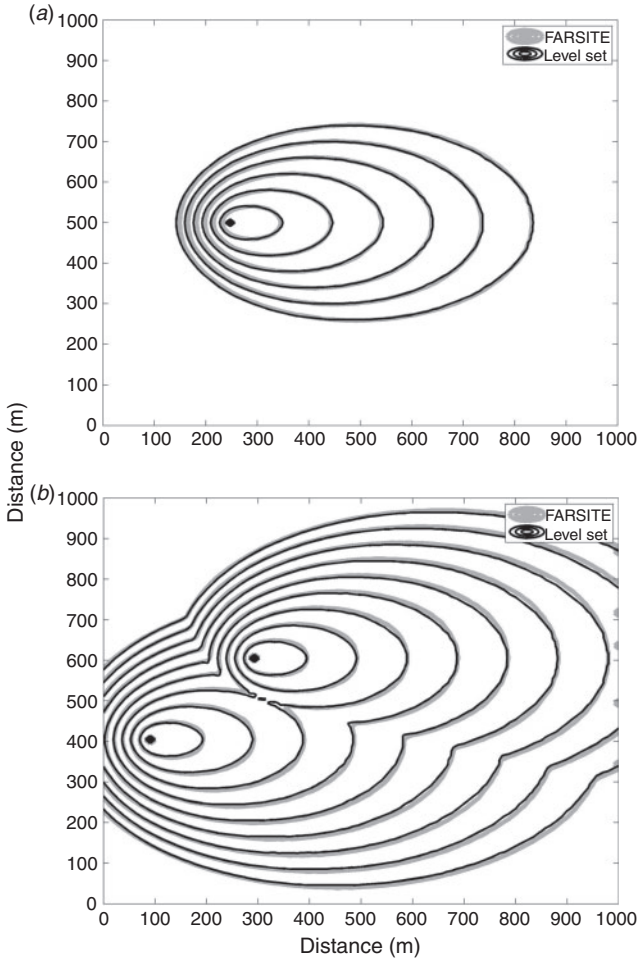

Fig. 1. Expansion of fire lines in level set (black) and FARSITE (grey) grass fuel simulations. Wind speed: 18 km h^{-1} (at 10-m height) blowing from left to right. Contours are separated by 180 s. Units of horizontal and vertical axes are metres.

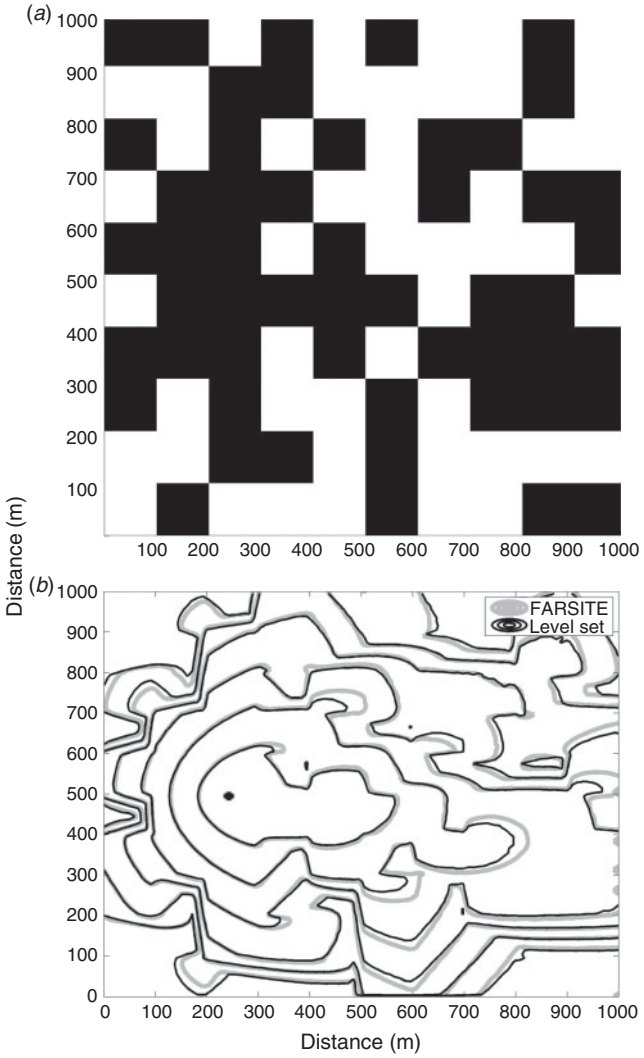

Fig. 2. (*a*) Random pattern of 100-m × 100-m fuel patches over the 1 × 1-km domain. Light and dark squares represent the grass and chamise fuel models respectively. (*b*) Fire contours at 600-s intervals over random fuel patches shown in (*a*). Wind is 18 km h^{-1} at 10 m blowing from left to right.

domain. The pattern of fuel types is shown in Fig. 2*a*. Despite the sharp boundaries between fuel types, the pattern of spread was very similar between the models (Fig. 2*b*). The difference between the two models in the perimeter of the first isochrone is ~2%, which is maintained (Fig. 3*a*) until the contours begin to intercept the domain boundaries and both of the estimated perimeters diminish (owing to exclusion of the boundary). Both the perimeter and final burned area in LS are ~2% larger than in FS, as shown in Fig. 3*a* and 3*b* respectively.

Fuel breaks (i.e. non-burnable patches on the landscape) provide a different challenge for the level set method, as they create a sharp gradients in the level set function between unignitable areas, where the level set function is held constant, and fuels surrounding the fuel break where the value of the level set function changes as the fire front passes. Fire spread in the grass fuel around a large (300 × 300-m) non-burnable patch is illustrated by the contours in Fig. 4*a*. Wind was again from left to right at 18 km h^{-1} and the ignition point was located at (250 m, 500 m). The match between fire lines and burned areas (Fig. 4*b*) generated by the two models is close, with a final difference in burned area of ~5%.

A more complex case is shown in Fig. 5*a*, which indicates TOA contours, at 240-s intervals, of fire spreading through an array of the custom grass fuel and 50 × 50-m non-burnable patches. In this case, the ignition location is at (275 m, 530 m). Although the contours of the two models overlap in the along-wind (left to right) direction through the central portion of the domain (i.e. along $y = 530$ m), the flanking contours generated by LS lag behind corresponding FS contours. This is confirmed by Fig. 5*b*, in which, after ignition, the burned area of the FS model is consistently 11–12% greater than the burned area of the LS model.

Interestingly, the difference between the isochrones decreased considerably when the superbee flux limiter was used instead of the default minmod limiter, with a final LS burned area that was only 3% less than the final FS burned area (not shown).

Increasing the resolution of the LS domain decreases the differences between LS and FS contours regardless of whether the minmod or superbee limiter is used. For example, using the

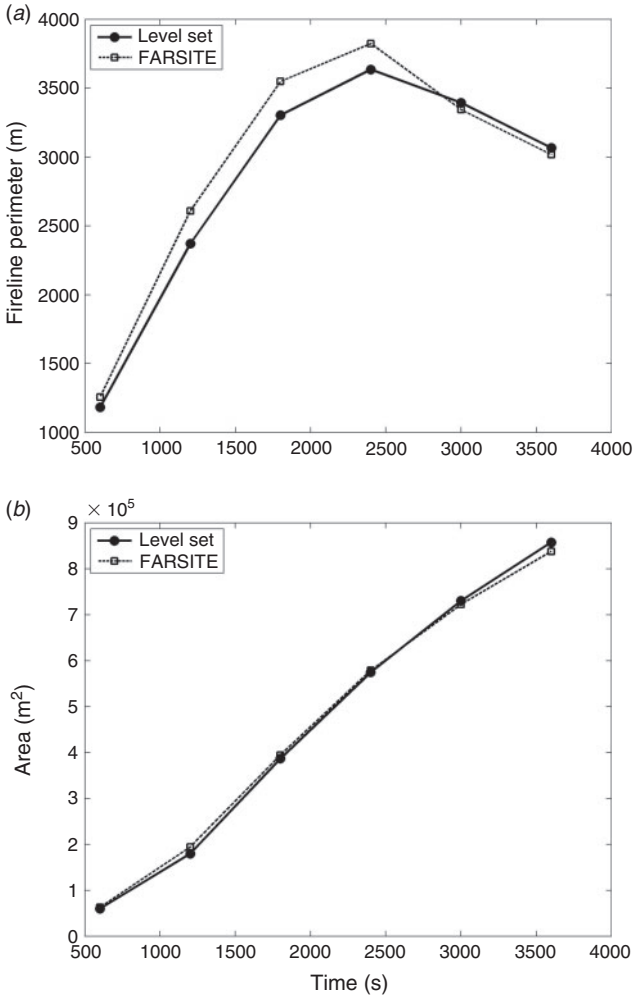

Fig. 3. Growth of fire line perimeter (*a*) and burned area (*b*) as fire travels over random fuel patches shown in Fig. 2*a*.

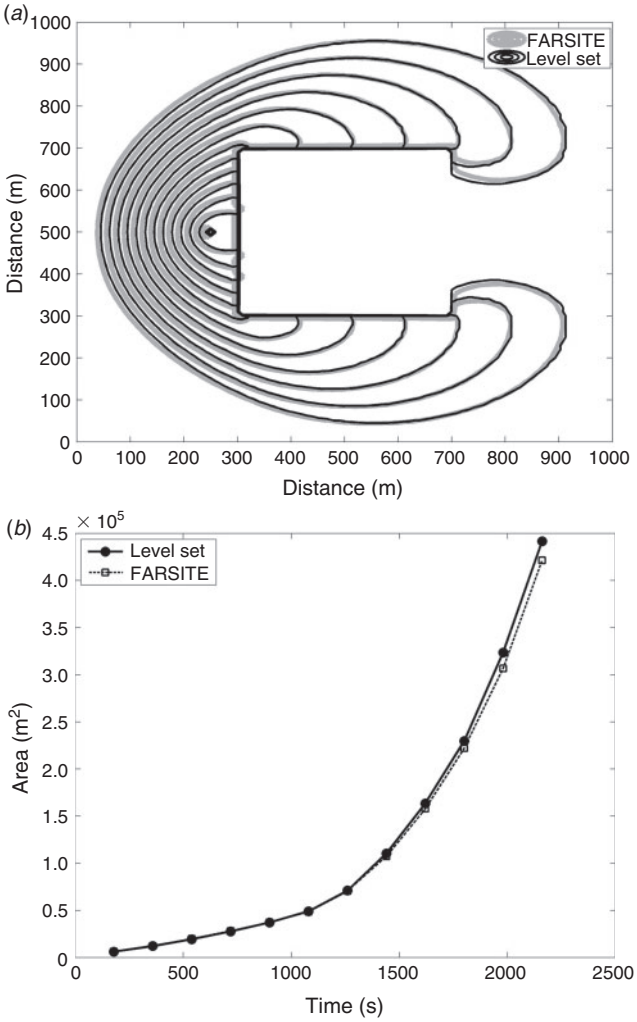

Fig. 4. (*a*) Fire contours at 180-s intervals in domain with large non-burnable patch (400 × 400 m) in the centre of the domain and grass fuel everywhere else. Wind is 18 km h^{-1} at 10 m blowing from left to right. (*b*) Burned area in grass fuel with large non-burnable patch.

minmod limiter, the correspondence between the two models is significantly improved when the resolution in LS is set to 2 m (Fig. 6*a*). The difference in burned areas is less than 3% at the final time-step of the simulation. The reason for this improvement in model agreement will be addressed in the Discussion section below.

Note that the configuration of this domain also tests the ability of the level set method to merge fire lines as they are separated by, and spread around, the unburnable patches. As mentioned, unlike the marker method, no special algorithms are required to model this phenomenon in LS, as it occurs naturally when the level set equation is solved.

Fire spread across a landscape with complex terrain

The topographical complexity of the domain was increased by adding a simulated, natural-looking landscape that was generated by applying a '1/*f*' filter to the fast Fourier transform (fft) of a random noise field. The inverse fast Fourier transform (ifft) of this filtered field generates a realistic fractal landscape (see e.g. Bourke 1997). Fig. 7*a* shows a three-dimensional plot of the landscape with complex terrain. Surface elevations range between 0 and 200 m with maximum elevation angles of ~85° from horizontal. As in previous simulations, wind is from left to right at 18 km h^{-1}, the terrain is covered with grass fuel, and the ignition point is located at (250 m, 500 m).

Time-of-arrival contours, spaced 300 s apart, from the landscape simulation using the minmod flux limiter are displayed in Fig. 7*b*. The corresponding contours of the two models match closely, although the LS contours have sections of greater curvature than those generated by FS. This leads to a final fire perimeter in LS that is ~6% greater (Fig. 8*a*), but a final burned area that is ~2% less (Fig. 8*b*) than those respective measures in FS.

Finally, we further increased the complexity of the complex-terrain simulation by changing the uniform grass surface fuel to the same pattern of randomly placed grass and chamise fuel patches that was used in the flat-terrain case of Fig. 2*a*. The pattern of fuel patches is shown in Fig. 2*a*. The ignition point, wind speed and direction were the same as the previous case. Time-of-arrival contours, 600 s apart, are shown in Fig. 9*a*,

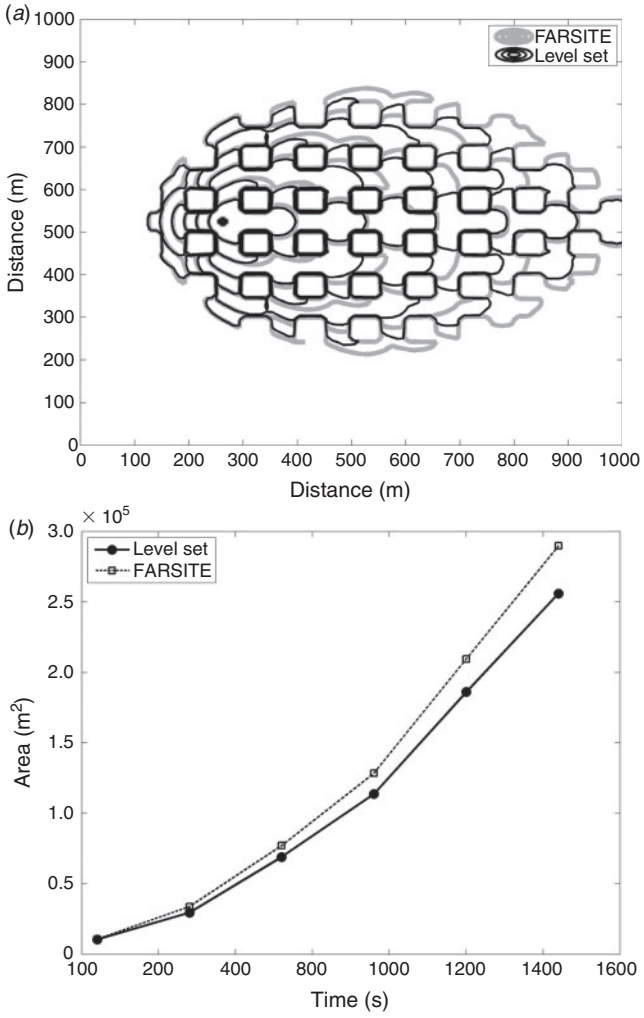

Fig. 5. (*a*) Fire contours at 240-s intervals in domain with multiple 50 × 50-m fuel breaks surrounded by grass on a flat terrain. Wind is 18 km h^{-1} at 10 m blowing from left to right. (*b*) Growth of burned area in grass fuel with multiple fuel breaks.

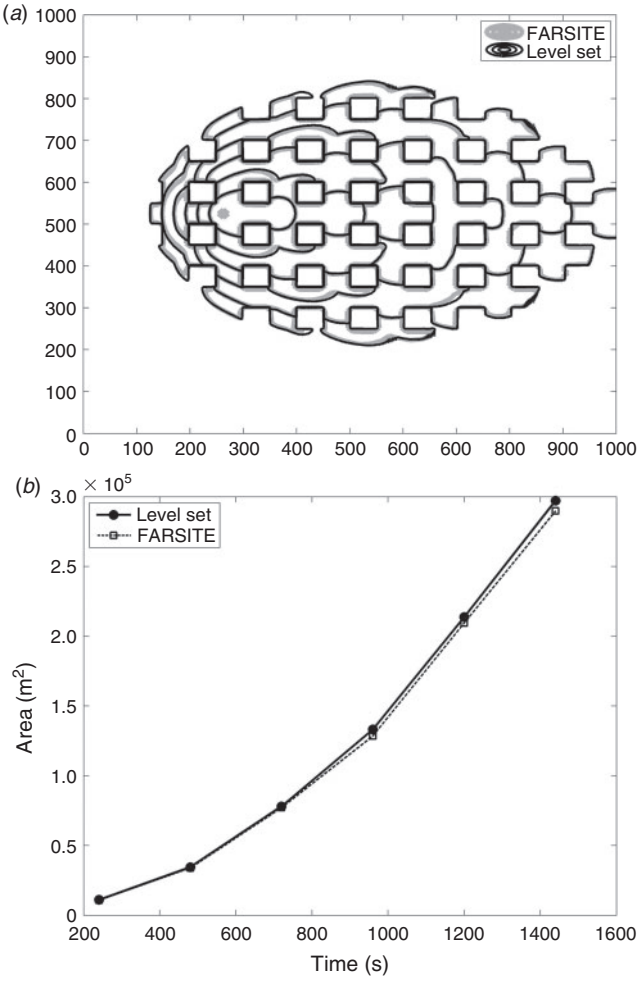

Fig. 6. (*a*) Fire contours at 240-s intervals in a high-resolution ($\Delta x = \Delta y = 2$ m) domain with multiple unignitable patches surrounded by grass fuel. This is the same as the case shown in Fig. 5*a*, which has a coarser grid resolution of $\Delta x = \Delta y = 10$ m. Wind is 18 km h^{-1} at 10 m blowing from left to right. (*b*) Corresponding growth of burned area.

where it is apparent that the LS and FS models, although similar, show more pronounced differences than in previous cases. In general, the LS model, using the minmod limiter, lags FS in the later contours. The greatest difference between the models occurs approximately half-way through the simulation, where burned area in the LS simulation is ~16% less than that of the FS simulation (Fig. 9*b*).

As shown in Fig. 10*a*, repeating the simulation with complex terrain and grass and chamise fuels but using the superbee flux limiter improves the correspondence between the two models, especially in the crosswind direction. In this case, the final burned area in LS is only ~3% larger than in FS (Fig. 10*b*).

Discussion

Using either the minmod or superbee flux limiters, there seems to be no significant difference between the solutions of the Eulerian and Lagrangian methods for simple cases involving flat terrain or uniform slope.

One of the larger discrepancies between the LS and FS models occurred when the model domain comprised a checkerboard pattern of unburnable patches (Fig. 5*a*). However, there was significant improvement in model agreement when the superbee flux limiter was used rather than the default minmod limiter. This may be explained by the fact that the superbee limiter is known to provide more accurate solutions near sharp boundaries (Pietrzak 1998), such as those that occur at the interface between non-burnable areas (i.e. areas of constant ϕ_{LS}) and neighbouring fuel patches. Technical details regarding flux limiters are given in Appendix 1.

Increasing the mesh resolution to 2 m in the above case brought the models into almost perfect agreement (Fig. 6*a*). This is because spatial resolution of the fire front, as it curves around and between the non-burnable areas, affects the rate of spread in the LS model. At 10-m resolution, the space between non-burnable patches in the checkerboard simulation spans only five grid cells. Thus, the gradients $\partial\phi_{LS}/\partial x$ and $\partial\phi_{LS}/\partial y$ are coarsely resolved, affecting the rate of change of ϕ_{LS} by Eqn 1.

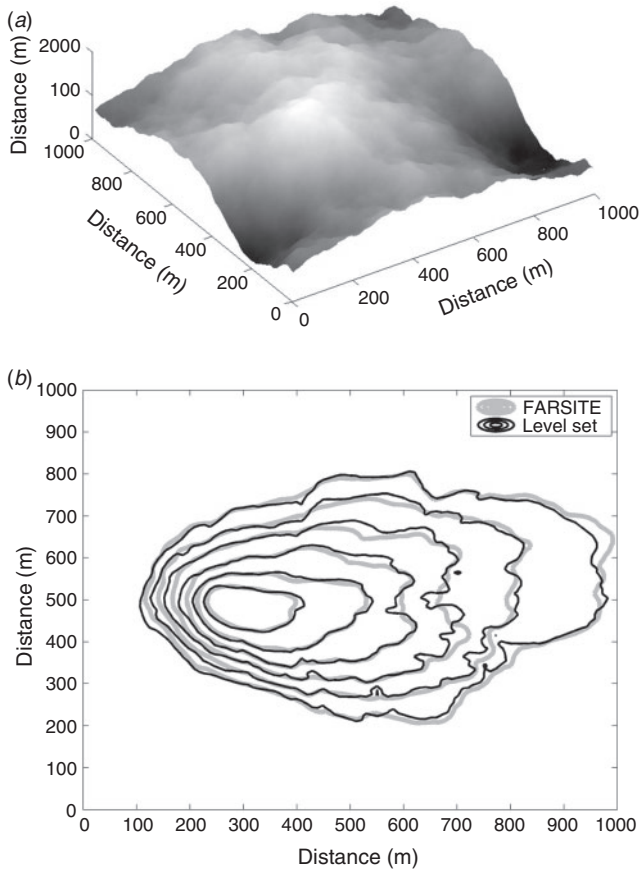

Fig. 7. (*a*) Surface plot of artificial landscape. (*b*) Corresponding fire-line contours for grass fuel. Wind is 18 km h^{-1} at 10 m blowing from left to right.

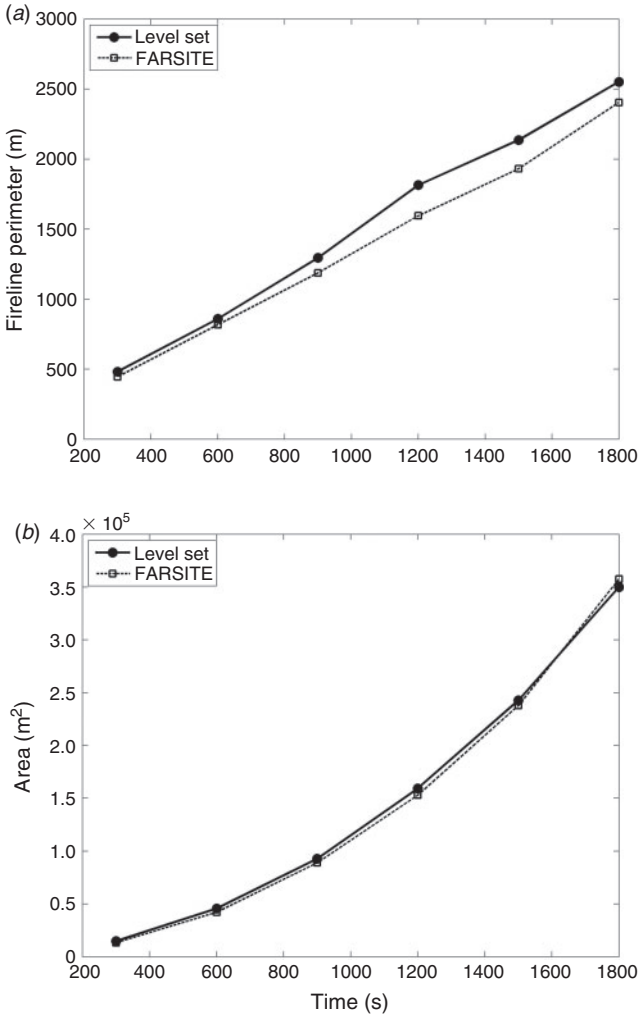

Fig. 8. (*a*) Fire perimeter growth in the grass fuel over the landscape domain. (*b*) Growth in burned area.

Increasing the resolution of the LS domain is analogous to the procedure in Lagrangian methods, such as FS, where the number of vertices per unit length of fire line is adjusted to be denser in areas of high fire-line curvature (Finney 1998). This suggests that level set simulations of fire spread might be improved by incorporating adaptable meshes that increase in resolution near areas of high front curvature. Of relevance to this study is the fact that both models could be made to agree quite well for this domain by using the superbee limiter or by increasing the LS spatial resolution or both.

Despite sharp boundaries between the randomly placed patches of two different fuel types, there were only minor discrepancies between the corresponding fire-line contours of the models (Figs 2*b*, 4*a*, and 6*a*). The front in the LS model slightly lags behind that of the FS model when the fire front curves around and between patches of the chamise fuel, in which the spread rate is lower.

For the real-world application of fire spread simulations, the most relevant comparisons are those of the landscape simulations. Considering its spatial scale (1 km), the artificial landscape shown in Fig. 7*a* is probably an extreme example of topographical variation. Despite this, the difference between fire contours is small in the case of a uniform fuel type (Fig. 7*b*), with only a 2% difference between burned areas in the two models (Fig. 8*b*).

Although there were only minor differences between the contours produced by the LS and FS model in the case of randomly placed fuel patches on a flat terrain (Fig. 2*b*), adding the same fuel pattern to the landscape with complex terrain seems to exaggerate these differences, giving the greatest discrepancies between the LS and FS contours of all the cases presented here. In this case in particular, relatively small dissimilarities at the initial stages of the simulation seem likely to become exaggerated as time progresses. For example, at 600 s, there is a slight mismatch between the contours in the region between the points (400 m, 380 m) and (550 m, 500 m) in Fig. 9*a*. This difference seems to increase as the LS fire line lags behind the FS at successive contours from left to right.

There is improvement in model agreement in the patched-fuel landscape domain, though, when the superbee flux limiter is used (Fig. 10*a* and 10*b*). Part of this improvement may stem from the ability of the superbee limiter to handle sharp boundaries or gradients, such as those produced by the combination of changing fuel types and steep slopes.

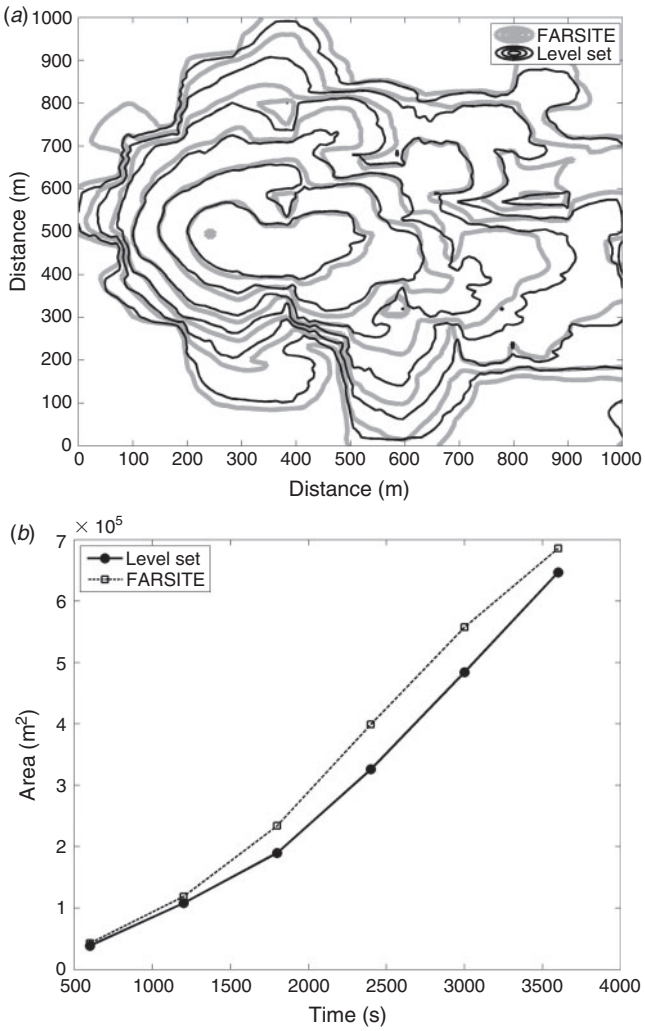

Fig. 9. (*a*) Time of arrival contours, at 600-s intervals, for the landscape domain (Fig. 7*a*) covered with random fuel patches (Fig. 2*a*). The minmod flux limiter was used in this case. Wind is 18 km h^{-1} at 10 m blowing from left to right. (*b*) Growth in burned area.

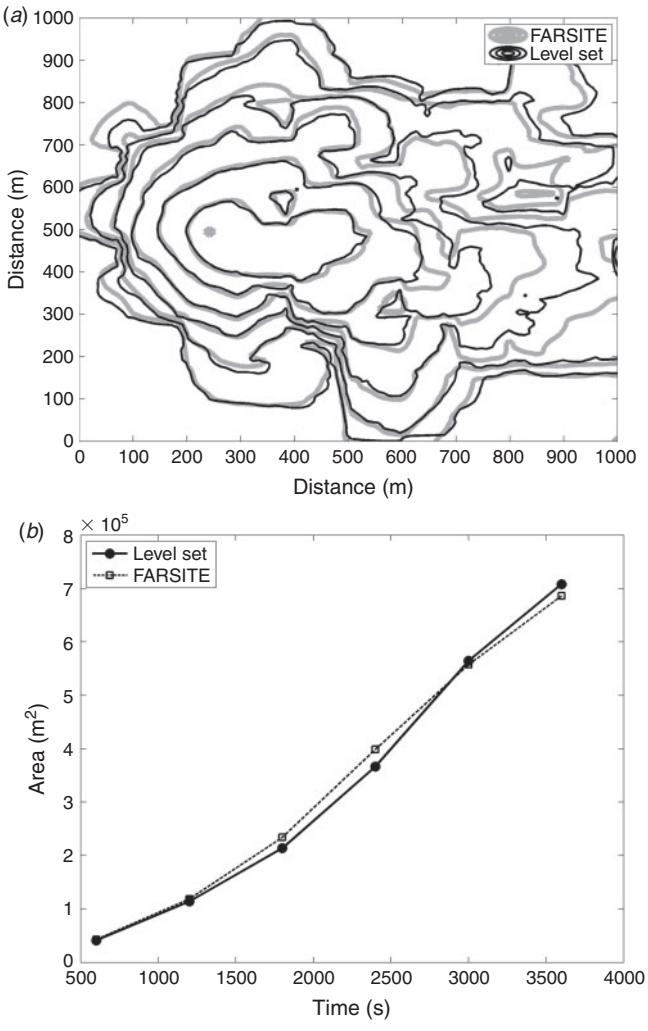

Fig. 10. (*a*) Time of arrival contours, at 600-s intervals, for the landscape domain (Fig. 7*a*) covered with random fuel patches (Fig. 2*a*). The superbee flux limiter was used in this case. Wind is 18 km h^{-1}.

Additional consideration is that, in the WFDS implementation of LS, slope is defined by Eqns A4 and A5 in Appendix 1. Thus, the calculation of slope is influenced by horizontal resolution. For example, a height difference of 30 m over adjacent cells gives a slope of 1.5 (50°) when the horizontal cell dimension is 10 m, but a slope of 3 (71°) when the horizontal dimension is 5 m. In contrast, slope is defined separately from the height of the landscape in FS; therefore, the values of slope do not change with resolution of the landscape.

Despite the improvement in this case and in the case of multiple fuel breaks, using the superbee limiter does not guarantee better correspondence with FS in all scenarios. For example, between the minmod and superbee limiters, there is little to no difference in LS output for the simple, flat-terrain cases. It should also be noted that there are several other flux-limiter functions, as well as solution methods, available to numerically solve the level set function. It is possible that a different combination of solver and flux limiter could improve correspondence in these cases.

Similarly, increasing the resolution of the LS grid may or may not improve the similitude between results of the LS and FS models. Although increasing the grid resolution of the LS model significantly improves the correspondence of contours in the case of multiple fuel breaks (Fig. 5*a* versus Fig. 6*a*), this is not true for the patchy landscape domain, where decreasing the LS grid cell dimension to 5 m generated little improvement over the 10-m resolution case (not shown).

The difference in results that may occur when using different resolutions or solvers underscores an important point: regardless of fire model, simulations used in real-world applications should be executed repeatedly, for a given scenario, while varying key parameters in order to evaluate the sensitivity of outcomes to the parameter space. The range of uncertainty inherent in fire spread models (e.g. the Rothermel model), and the sensitivity of results to variations in key parameters suggest that, as in weather

forecasting, ranges or probabilities of results are more appropriate than specific predictions.

Aside from the different underlying approaches between the two models (i.e. Eulerian versus Lagrangian), there are additional differences that may have affected the comparison. For example, given that the FS source code is not available, it is likely that there were differences between the LS and FS implementations of the underlying elliptical spread model. In addition, the two models handle landscape slopes differently, with slope being calculated in LS, and thus sensitive to grid cell size, but predefined and unchanging in FS. Despite these differences, the correspondence between the output of the LS and FS models was reasonably consistent. Therefore, although level set and Lagrangian marker approaches may be regarded as different models (Rehm and McDermott 2009), the results presented here suggest that, for the purpose of simulating wildland fire spread, they are similar enough in most cases to be considered interchangeable.

Finally, it should be clear that these simulations do not constitute validation of the WFDS-LS, or FS, models of fire spread, as the goal of the present paper is simply to compare the outcomes of corresponding scenarios separately modelled within Eulerian and Lagrangian frameworks. Whether or not the elliptical fire line shape and rate of spread models are appropriate for all cases of wildland fire spread is a topic for other studies. Confirming the strong similarity between simulations using the two models will support subsequent work in which we compare the simulations using the WFDS-PB model and WFDS-LS with different degrees of coupling (i.e. feedback) between the fire and atmosphere. This follow-on comparison will explore the implication on model outcomes of not including coupled physical processes in simple fire front propagation models such as WFDS-LS (as implemented here) and FS. Fire behaviours of interest are fire-line acceleration for a period after ignition or up a drainage, the response of the fire line to changes in the ambient wind, fire-line merging, fire spread over hill or ridge crests, and fire-line propagation through and around fuel treatments and fire breaks.

Conclusion

Although there is a mathematical equivalence between the Eulerian and Lagrangian methods of advancing a fire front, there is a question of whether or not equivalent fire spread models will give the same results when numerically implemented within these two frameworks. A suite of simulations of increasing complexity was created to compare these frameworks as instanced by the WFDS-LS and FARSITE models. For simple scenarios, such as flat terrain and uniform fuel type, the two models give virtually identical results. Although there are noticeable differences between the results of both models in more complex cases, such as variable terrain and fuels, these differences may be minimised by the choice of solvers or resolution used in the WFDS-LS model.

Acknowledgements

Funding for this work was provided primarily by Joint Venture Agreement 12-JV-11261987–102 between the USFS Pacific Wildland Fire Sciences Laboratory and Colorado State University and Joint Fire Science Project 14–1-01–18.

References

Anderson HE (1983) Predicting wind-driven wildland fire size and shape. USDA Forest Service, Intermountain Forest and Range Experiment Station, Research Paper INT-305. (Ogden, UT)

Andrews PL (2012) Modeling wind adjustment factor and midflame wind speed for Rothermel's surface fire spread model. USDA Forest Service, Rocky Mountain Research Station, General Technical Report RMRS-GTR-266. (Fort Collins, CO) Available at http://firemodels.org [Verified 6 July 2015]

Andrews PL (2014) Current status and future needs of the BehavePlus fire modeling system. *International Journal of Wildland Fire* **23**, 21–33. doi:10.1071/WF12167

Barber J, Bose C, Bourlioux A, Braun J, Brunelle E, Garcia T, Hillen T, Ong B (2008) Burning issues with Prometheus – the Canadian wildland and fire growth simulation model. *Canadian Applied Mathematics Quarterly* **16**, 337–378.

Bourke P (1997) Frequency synthesis of landscapes (and clouds). Available at http://paulbourke.net/fractals/noise/[Verified 6 July 2015]

Coen J (2013) WRF-Fire: coupled weather–wildland fire modeling with the Weather Research and Forecasting Model. *Journal of Applied Meteorology and Climatology* **52**, 16–38. Available at http://journals.ametsoc.org/doi/pdf/10.1175/JAMC-D-12-023.1 [Verified 6 July 2015]

Fendell FE, Wolff MF (2001) Wind-aided fire spread. In 'Forest fires – behavior and ecological effects.' (Eds E Johnson, K Miyanishi) pp. 171–223 (Academic Press: San Diego, CA)

Ferziger JH, Peric M (2002) 'Computational methods for fluid dynamics', 3rd edn. (Springer-Verlag: Berlin)

Finney MA (1998) FARSITE: Fire Area Simulator – model, development and evaluation. USDA Forest Service, Rocky Mountain Research Station, Research Paper RMRS-RP-4. (Fort Collins, CO)

Finney MA (2004) FARSITE: Fire Area Simulator – model, development and applications. USDA Forest Service, Rocky Mountain Research Station, Paper RMRS-RP-4 Revised. (Fort Collins, CO) Available at http://www.fs.fed.us/rm/pubs/rmrs_rp004.pdf [Verified 6 July 2015]

Heinsch FA, Andrews PL (2010) BehavePlus fire modeling system, version 5.0: design and features. USDA Forest Service, Rocky Mountain Research Station, General Technical Report RMRS-GTR-249. (Fort Collins, CO)

Kundu PK, Cohen IM (2008) 'Fluid mechanics', 4th edn. (Academic Press: San Diego, CA)

Lautenberger C (2012) Modeling wildland fire spread using an Eulerian level set method and high-resolution numerical weather prediction. Technical report. (Reax Engineering, Inc.: Berkeley, CA). Available at http://reaxengineering.com/ [Verified 6 July 2015]

Mallet V, Keyes DE, Fendell FE (2009) Modeling wildland fire propagation with level set methods. *Computers & Mathematics with Applications* **57**, 1089–1101. doi:10.1016/J.CAMWA.2008.10.089

Mandel J, Beezley JD, Kochanski AK (2011) Coupled atmosphere–wildland fire modeling with WRF 3.3 and SFIRE 2011. *Geoscientific Model Development* **4**, 591–610. doi:10.5194/GMD-4-591-2011

Mell WE, Jenkins MA, Gould J, Cheney P (2007) A physics-based approach to modeling grassland. *International Journal of Wildland Fire* **16**, 1–22. doi:10.1071/WF06002

Pietrzak J (1998) The use of TVD limiters for forward-in-time upstream-biased advection schemes in ocean modeling. *Monthly Weather Review* **126**, 812–830. doi:10.1175/1520-0493(1998)126<0812:TUOTLF>2.0.CO;2

Quintiere JG (2006) 'Fundamentals of fire phenomena.' (John Wiley & Sons: Chichester, UK)

Rehm R, McDermott R (2009) Fire-front propagation using the level set method. NIST Technical Note 1611. (Gaithersburg, MD). Available at http://fire.nist.gov/bfrlpubs/fire09/art023.html [Verified 6 July 2015]

Richards GD (1990) An elliptical growth model of forest fire fronts and its numerical solution. *International Journal for Numerical Methods in Engineering* **30**, 1163–1179. doi:10.1002/NME.1620300606

Rothermel RC (1972) A mathematical model for predicting fire spread in wildland fuels. USDA Forest Service, Intermountain Forest and Range Experiment Station, Research Paper INT-115 (Ogden, UT). Available at http://www.treesearch.fs.fed.us/pubs/32533 [Verified 6 July 2015]

Sethian JA (1992) 'Level set methods and fast-marching methods', 2nd edn. (Cambridge University Press: Cambridge, UK)

Sethian JA (1997) Tracking interfaces with level sets. *American Scientist* **85**, 254–263.

Weise DR, Regelbrugge J (1997) Recent chaparral fuel modeling efforts. Available at http://web.physics.ucsb.edu/~complex/research/hfire/fuels/refs/weiseregel1997.pdf [Verified 6 July 2015]

Wilson R (1980) Reformulation of forest fire spread equations in SI units. USDA Forest Service, Intermountain Forest and Range Experiment Station, Research Paper INT-292. (Ogden, UT) Available at http://www.fs.fed.us/rm/pubs_int/int_rn292.pdf [Verified 6 July 2015]

Appendix 1. Implementing the elliptical fire spread model in WFDS-LS

The methodology described below reproduces (in an Eulerian framework) the approach used in the Lagrangian-based fire front-tracking model FARSITE (Finney 2004). This approach makes use of the Rothermel (1972) surface fire spread rate formulae and the assumption that a surface fire spreading from a point under certain wind, slope and vegetation conditions does so with an ellipse-shaped fire front with, for a given wind speed, a fixed length-to-breadth ratio (Richards 1990).

In WFDS, model domains and parameters are prescribed within a text file, usually referred to as the 'input' file, that is read and interpreted before the execution of a simulation. Currently, LS does not contain the Rothermel model for the calculation of no-wind, no-slope spread rate (R_0). To describe a fuel for the level set model, R_0 is calculated using Behave *v.* 5.0 (Heinsch and Andrews 2010) and entered in the input file, along with the packing ratio, β, surface area-to-volume ratio, σ (cm^{-1}) and fuel height, h (m). The latter three parameters are used in the calculation of midflame wind speed (U_{mf}) and the wind and slope coefficients (ϕ_{w} and ϕ_{s}). These coefficients are used to modify R_0 and obtain the local spread R. (Note that we retain the customary 'ϕ' notation for the wind and slope coefficients. These should not be confused with the level set field, ϕ_{LS}). The wind and slope coefficients were determined from laboratory measurements (Rothermel 1972) as functions of uniform vegetation, wind and slope conditions. In fact, the fire spread direction was aligned with either the wind direction or the change in slope (no experiments were conducted with a combination of non-zero wind and slope). The wind and slope coefficients derived from the experimental data are (Wilson 1980):

$$\phi_{\mathrm{W}} = C(3.281U_{\mathrm{mf}})^{B}\left(\frac{\beta}{\beta_{\mathrm{op}}}\right)^{-E} \tag{A1}$$

$$\phi_{\mathrm{S}} = 5.275\beta^{-0.3}(\tan\Phi)^2$$

where:

$$\tan\Phi = \frac{\delta z}{\delta x} \text{ or } \frac{\delta z}{\delta y}$$

$$B = 0.15988\sigma^{0.54}$$

$$C = 7.47\exp(-0.8711\sigma^{0.55})$$

$$E = 0.715\exp(-0.01094\sigma)$$

$$\beta_{\mathrm{op}} = 0.20395\sigma^{-0.8189}$$

In general, the conditions to which the WFDS level set model (or FARSITE) is applied are such that the wind and slope are both non-zero and neither is aligned with the direction of fire spread. This requires an extension of the ϕ_{w} and ϕ_{s} point values to vectors with components in the x- and y-directions. For example, the wind coefficient is the vector

$$\boldsymbol{\phi}_{\mathrm{W}} = (\phi_{\mathrm{W},x}, \phi_{\mathrm{W},y}) = \mathrm{C}(3.281)^{\mathrm{B}}\left(\frac{\beta}{\beta_{\mathrm{op}}}\right)^{-\mathrm{E}} \times \left(\left|U_{\mathrm{mf},x}\right|^{B}\mathrm{sign}(U_{\mathrm{mf},x}), \left|U_{\mathrm{mf},y}\right|^{B}\mathrm{sign}(U_{\mathrm{mf},y})\right)$$

A similar approach is used to find the vector form of the slope coefficient:

$$\boldsymbol{\phi}_{\mathrm{S}} = (\phi_{\mathrm{S},x}, \phi_{\mathrm{S},y}) = 5.276\beta^{-0.3}\left(\left[\frac{\delta z}{\delta x}\right]^2, \left[\frac{\delta z}{\delta y}\right]^2\right)$$

The midflame wind vector is found using eqn 8 of Andrews (2012):

$$\boldsymbol{U}_{\mathrm{mf}} = \boldsymbol{U}_0\frac{1.83}{\ln\left(\frac{20+1.18h}{0.43h}\right)} \tag{A2}$$

where $\boldsymbol{U}_0$ is the wind vector at 6.1 m (20 feet) above ground level (AGL), h is fuel height (m) and the coefficients of h have been converted, here, to SI units. Note that, as in Andrews (2012) and Finney (2004), this formula is based on the assumption that the flame height above the fuel is equal to the height of the fuel. Only SI units are used in the physics-based WFDS (WFDS-PB) and LS models. In particular, wind speed has units of metres per second and, as required when using Eqn A2, is assumed to be at a height of 6.1 m above the ground. For consistency with LS, metric units (km h^{-1}) were used to prescribe wind speed in the FS simulations described above. However, in FS, if a wind speed is entered in metric units, it is assumed to be the speed at a height of 10 m AGL. That speed is divided by a factor of 1.15 to convert it to a wind speed at 6.1 m (Andrews 2012). Thus, a wind speed of 18 km h^{-1} in FS is equivalent to a wind speed of 4.3 m s^{-1} in LS (i.e. $18/1.15 \times 0.28$, where 0.28 converts km h^{-1} to m s^{-1}).

The surface fire spread rate, R, is found following Rothermel (1972) using the magnitude of the combined wind and slope coefficient vectors:

$$R = R_0(1 + \sqrt{(\boldsymbol{\phi}_{\mathrm{W}} + \boldsymbol{\phi}_{\mathrm{S}})\cdot(\boldsymbol{\phi}_{\mathrm{W}} + \boldsymbol{\phi}_{\mathrm{S}})}) \tag{A3}$$

To model topography, FS accepts files in grid-ASCII format, in which values at each grid point on a landscape are defined in a text file as a grid (matrix) of numbers. Elevations, slopes and aspects are each defined in different files. In LS, topography is created by defining obstructions (blocks) of varying elevations within the rectilinear grid of the domain. Slopes of a grid cell located at (i,j) are calculated as the first-order central difference of elevations in the x- and y-directions:

$$\left(\frac{\delta z}{\delta x}\right)_{i,j} = \frac{z_{i+1,j} - z_{i-1,j}}{2\Delta x} \tag{A4}$$

$$\left(\frac{\delta z}{\delta y}\right)_{i,j} = \frac{z_{i,j+1} - z_{i,j-1}}{2\Delta y} \tag{A5}$$

where $\frac{\delta z}{\delta x} \approx \frac{\partial z}{\partial x}$, $\frac{\delta z}{\delta y} \approx \frac{\partial z}{\partial y}$, and $z(x,y)$ is the terrain height (x,y). Note that, in LS, for any given horizontal resolution, the increments of slope are limited by the vertical resolution, Δz.

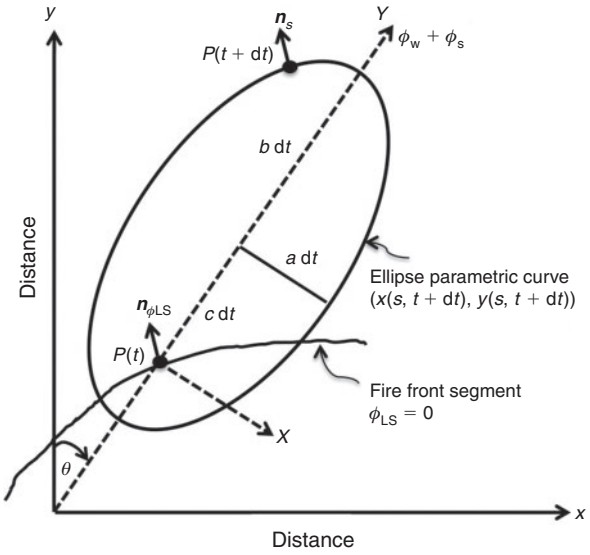

Fig. A1. Geometry of solution method. Point $P(t)$ is a point on the fire front at time t. The location of P at time $t + \mathrm{d}t$ is determined by assuming the fire front spreading from $P(t)$ is an ellipse with semi-major and semi-minor axes $a\ \mathrm{d}t$ and $b\ \mathrm{d}t$, respectively (see text). At time $t + \mathrm{d}t$ point $P(t)$ is located at $P(t + \mathrm{d}t)$. The direction of maximum spread, as a function of the local wind, terrain and vegetation at point $P(t)$ (see Eqn A3), is $\phi_w + \phi_s$. This direction is at a clockwise angle θ from the y axis of the computational grid. The actual spread rate at $P(t)$ depends on the direction of the vector normal to the fire front pointing in the direction of fire spread. This normal vector is denoted by $\boldsymbol{n}_{\phi LS}$ when computed in terms of the level set field and by $\boldsymbol{n}_s$ when computed in terms of the parameter s (see text). The parametric equation at time $t + \mathrm{d}t$ for the ellipse fire front spreading from $P(t)$ is $(x(s, t + \mathrm{d}t), y(s, t + \mathrm{d}t))$. The axes (x, y) correspond to the level set computational grid and the axes X, Y are for the ellipse (see Richards 1990).

Fig. A1 shows the geometry of the solution method. A point on the fire front at time t is denoted $P(t)$. The location of P at time $t + \mathrm{d}t$ is determined by assuming fire front spreads from $P(t)$ as an ellipse with semi-major and semi-minor axes ($a\ \mathrm{d}t$) and ($b\ \mathrm{d}t$) respectively. The formula for the length-to-breadth ratio, LB, of the elliptical fire front emanating from $P(t)$ is (Anderson 1983; Finney 2004):

$$LB = 0.936\exp(0.2566U) + 0.461\exp(-0.1548U) - 0.397 \tag{A6}$$

$$LB = \max(1, \min(LB, 8)) \tag{A7}$$

where the maximum constraint on LB, Eqn A7, matches that in Finney (2004). Note that this formula includes the influence of only the open wind speed, U, and does not address the effect of slope on the shape of the fire front. We use Finney's assumption (Finney 2004) that the effect of slope may be accounted for by creating a *virtual* midflame wind speed. Here, this is extended to a vector form:

$$\boldsymbol{U}_{\mathrm{virtual}} = 0.3048\left[\frac{1}{C}\left(\frac{\beta}{\beta_{\mathrm{op}}}\right)^{E}\right]^{\frac{1}{B}}(\phi_{\mathrm{S},x}, \phi_{\mathrm{S},y})$$

where ϕ_s has been substituted for ϕ_w in the point function Eqn A1, which was then solved for U. The sum of the $\boldsymbol{U}_{\mathrm{mf}}$ and $\boldsymbol{U}_{\mathrm{virtual}}$ vectors is referred to as the 'effective' wind vector. The magnitude of the effective wind vector is used for U in Eqn A6.

The heading-to-backing fire spread rate ratio, HB and spread rates that determine the elliptical axes are calculated as in Finney (2004):

$$HB = \left(LB + \sqrt{LB^2 - 1}\right) \Big/ \left(LB - \sqrt{LB^2 - 1}\right)$$

$$a = \frac{b}{LB}$$

$$b = \frac{1}{2}\left(R + \frac{R}{HB}\right)$$

$$c = b - \frac{R}{HB}$$

where a and b are the spread rates corresponding to the semi-major and semi-minor axes respectively, c is the spread rate between the ignition point $P(t)$ in Fig. A1 (i.e. the initial focus) and the centre of the ellipse, and R is the surface fire spread rate (Eqn A3) in the direction determined by the combined wind and slope coefficient vectors ($\phi_w + \phi_s$), as shown in Fig. A1. The head, flank and back fire spread rates for an ellipse with these properties are $b + c$, a, and $b - c$ respectively (Richards 1990).

Rate of spread vector components in the x- and y-directions for point $P(t)$ in Fig. A1 are computed as:

$$R_x = D\left[a^2\cos\theta(x_s\sin\theta + y_s\cos\theta) - b^2\sin\theta(x_s\cos\theta - y_s\sin\theta)\right] + c\sin\theta \tag{A8}$$

$$R_y = D\left[-a^2\sin\theta(x_s\sin\theta + y_s\cos\theta) - b^2\cos\theta(x_s\cos\theta - y_s\sin\theta)\right] + c\cos\theta \tag{A9}$$

where

$$D = \left[a^2(x_s\sin\theta + y_s\cos\theta)^2 + b^2(x_s\cos\theta - y_s\sin\theta)^2\right]^{-\frac{1}{2}}$$

Note that Finney (2004) and Richards (1990) have different values for D; we have followed Richards here. The quantities x_s and y_s are related to the components of the vector normal to elliptical fire front, $\boldsymbol{n}_s$, as defined parametrically by the curve $x(s, t)$, $y(s, t)$ (see Fig. A1). This normal vector pointing in the direction of fire spread is:

$$\boldsymbol{n}_s = (y_s, -x_s) = \left(\frac{\partial y}{\partial s}, -\frac{\partial x}{\partial s}\right)$$

In Fig. A1, the normal vectors $\boldsymbol{n}_{\phi LS}$ at $P(t)$ and $\boldsymbol{n}_s$ at $P(t + \mathrm{d}t)$ point in the same direction and define the spread rate components (Eqns A8 and A9) by specifying the location of $P(t)$ on an elliptical fire front (e.g. head fire versus flank fire). The normal

vector at $P(t)$ pointing in the direction of fire spread, as determined by the level set field, is:

$$\boldsymbol{n}_{\phi\mathrm{LS}} = \left(-\frac{\partial\phi_{\mathrm{LS}}}{\partial x}, -\frac{\partial\phi_{\mathrm{LS}}}{\partial y}\right)$$

where the negative signs are due to the fact that unburned and burned values of ϕ_{LS} are -1 and 1 respectively in WFDS-LS (this was done for visualisation purposes). Because x_s and y_s are in the numerator and denominator of the spread rate equations (Eqns A8 and A9) and the components of $\boldsymbol{n}_s$ and $\boldsymbol{n}_{\mathrm{LS}}$ are proportional to each other, the value of x_s or y_s in the spread rate equations can be replaced by its counterpart in $\boldsymbol{n}_{\mathrm{LS}}$.

The angle θ in the equations above is the azimuth (compass angle, or angle in the clockwise direction from the positive y axis) of the direction of the spread rate as determined by the wind and slope coefficient vectors (assumed to be the direction of maximum spread rate). This angle is determined by first using the two-argument arctangent function,

$$\theta = \mathrm{atan2}\left[\left(\phi_{\mathrm{W},y} + \phi_{\mathrm{S},y}\right) + \left(\phi_{\mathrm{W},x} + \phi_{\mathrm{S},x}\right)\right]$$

and then converting θ to a compass angle by the following operations:

$$\theta = \frac{\pi}{2} - \theta$$

$$\theta = 2\pi + \theta, \quad \text{if } \theta < 0$$

Eqn 1 is solved in the horizontal (x–y) plane only. At grid points where $|slope| > 0$, rates of fire spread in the x- and y-directions are projected onto the horizontal plane by multiplication with the cosine of slope angle (from horizontal) in the respective directions.

The numerical procedure for solving the level set Eqn 1 is described in Rehm and McDermott (2009). We provide a brief outline below.

Values of ϕ_{LS} are initialised to -1 throughout the domain. Ignition point(s) are prescribed a value of $+1$ at the appropriate time(s). As the fire front moves past a location, the value of the grid point will change from -1 to $+1$ over a time interval determined by the rate of fire spread.

At time t^n, gradients of ϕ_{LS} at the grid locations (i, j) are computed as central differences (here and below we omit the subscript 'LS' to simplify the notation):

$$\left(\frac{\delta\phi}{\delta x}\right)^n_{i,j} = \frac{\phi^n_{i+1,j} - \phi^n_{i-1,j}}{2\Delta x}$$

$$\left(\frac{\delta\phi}{\delta y}\right)^n_{i,j} = \frac{\phi^n_{i,j+1} - \phi^n_{i,j-1}}{2\Delta y}$$

where $\delta\phi/\delta x \approx \partial\phi/\partial x$ and $\delta\phi/\delta y \approx \partial\phi/\partial y$.

A flux-limiting scheme is used to constrain the spatial derivatives to physically realistic values. The following example of the use of a flux-limiting scheme is adapted from Rehm and McDermott (2009). The gradient of the function, ϕ, along the x-direction at the node (i, j) of the computational mesh is:

$$\frac{\delta\phi}{\delta x} = \frac{\phi_{\mathrm{east}} - \phi_{\mathrm{west}}}{\Delta x} \tag{A10}$$

where ϕ_{west} and ϕ_{east} are the mesh cell faces to the left and right respectively of the node. To find the value of ϕ_{east}, for instance, the data ratio, r, is computed first:

$$r = \begin{cases} \dfrac{\Delta\phi_{(\mathrm{upwind})}}{\Delta\phi_{(\mathrm{local})}} & \text{if } \phi_{(\mathrm{local})} \neq 0 \\ 0 & \text{if } \phi_{(\mathrm{local})} = 0 \end{cases}$$

where

$$\Delta\phi_{(\mathrm{upwind})} = \phi_{i,j} - \phi_{i-1,j}$$

$$\Delta\phi_{(\mathrm{local})} = \phi_{i+1,j} - \phi_{i,j}$$

The value of ϕ_{east} is then computed by:

$$\phi_{\mathrm{east}} = \phi_{i,j} + \frac{1}{2}B(r)\left[\phi_{i+1,j} - \phi_{i,j}\right] \tag{A11}$$

where $B(r)$ is one of three flux-limiting functions currently available in WFDS:

$$B(r) = 0 \text{ first-order upwinding}$$

$$B(r) = \max(0, \min(1, r)) \text{ minmod}$$

$$B(r) = \max(0, \min(2r, 1), \min(r, 2)) \text{ superbee}$$

Thus, in cases of a sharp gradient, where $\Delta\phi_{(\mathrm{upwind})} \ll \Delta\phi_{(\mathrm{local})}$, the minmod and superbee limiters diminish the contribution of the local variation, moving Eqn A11 toward a first-order upwind solution.

The numerical solution of the level set equation at time t^n is computed by a predictor-corrector scheme that is second-order accurate in space and time:

$$\phi'_{i,j} = \phi^n_{i,j} - \left(R_x\frac{\delta\phi}{\delta x} + R_y\frac{\delta\phi}{\delta y}\right)\Delta t$$

$$\phi^{n+1}_{i,j} = \frac{1}{2}\phi^n_{i,j} + \frac{1}{2}\left[\phi'_{i,j} - \left(R_x\frac{\delta\phi'}{\delta x} + R_y\frac{\delta\phi'}{\delta y}\right)\Delta t\right]$$

The time step, Δt, is adjusted at each iteration so that a conservative Courant–Friedrichs–Lewy (CFL) condition:

$$R_{\max} = \left(\frac{\Delta t}{\min(\Delta x, \Delta y)}\right) = 0.25$$

is maintained, where $R_{\max}$ is the maximum rate of spread predicted within the entire domain.